4.2.3. X-ray absorption spectra (by D. C. Creagh)

4.2.3.1. *Introduction*

4.2.3.1.1. *Definitions*

This section deals with the manner in which the photon scattering and absorption cross sections of an atom varies with the energy of the incident photon. Further information concerning these cross sections and tables of the X-ray attenuation coefficients are given in Section 4.2.4. Information concerning the anomalous-dispersion corrections is given in Section 4.2.6.

When a highly collimated beam of monoenergetic photons passes through a medium of thickness t, it suffers a decrease in intensity according to the relation

$$I = I_0 \exp(-\mu_l t), \tag{4.2.3.1}$$

where μ_l is the linear attenuation coefficient. Most tabulations express μ_l in c.g.s. units, μ_l having the units cm^{-1}.

An alternative, often more convenient, way of expressing the decrease in intensity involves the measurement of the mass per unit area m_A of the specimen rather than the specimen thickness, in which case equation (4.2.3.1) takes the form

$$I = I_0 \exp[-(\mu/\rho)m_A], \tag{4.2.3.2}$$

where ρ is the density of the material and (μ/ρ) is the mass absorption coefficient. The linear attenuation coefficient of a medium comprising atoms of different types is related to the mass absorption coefficients by

$$\mu_l = \rho \sum_i g_i (\mu/\rho)_i, \tag{4.2.3.3}$$

where g_i is the mass fraction of the atoms of the ith species for which the mass absorption coefficient is $(\mu/\rho)_i$. The summation extends over all the atoms comprising the medium. For a crystal having a unit-cell volume of V_c,

$$\mu_l = \frac{1}{V_c} \sum \sigma_i, \tag{4.2.3.4}$$

where σ_i is the photon scattering and absorption cross section. If σ_i is expressed in terms of barns/atom then V_c must be expressed in terms of Å^3 and μ_l is in cm^{-1}. (1 barn $= 10^{-28}$ m^2.)

The mass attenuation coefficient μ/ρ is related to the total photon–atom scattering cross section σ according to

$$\begin{aligned}\frac{\mu}{\rho}(\text{cm}^2/\text{g}) &= (N_\text{A}/M)\sigma\,(\text{cm}^2/\text{atom}) \\ &= (N_\text{A}/M) \times 10^{-24}\sigma\,(\text{barns/atom}),\end{aligned} \tag{4.2.3.5}$$

where N_A = Avogadro's number $= 6.0221367\,(36) \times 10^{23}$ atoms/gram atom (Cohen & Taylor, 1987) and M = atomic weight relative to $M(^{12}\text{C}) = 12.0000$.

4.2.3.1.2. *Variation of X-ray attenuation coefficients with photon energy*

When a photon interacts with an atom, a number of different absorption and scattering processes may occur. For an isolated atom at photon energies of less than 100 keV (the limit of most conventional X-ray generators), contributions to the total cross section come from the photo-effect, coherent (Rayleigh) scattering, and incoherent (Compton) scattering.

$$\sigma = \sigma_\text{pe} + \sigma_R + \sigma_C. \tag{4.2.3.6}$$

The relation between the photo-effect absorption cross section σ_pe and the X-ray anomalous-dispersion corrections will be discussed in Section 4.2.6.

The magnitudes of these scattering cross sections depend on the type of atom involved in the interactions and on the energy of the photon with which it interacts. In Fig. 4.2.3.1, the theoretical cross sections for the interaction of photons with a carbon atom are given. Values of σ_pe are from calculations by Schofield (1973), and those for Rayleigh and Compton scattering are from tabulations by Hubbell & Øverbø (1979) and Hubbell (1969), respectively. Note the sharp discontinuities that occur in the otherwise smooth curves. These correspond to photon energies that correspond to the energies of the K and L_I L_II L_III shells of the carbon energies. Notice also that σ_pe is the dominant interaction cross section, and that the Rayleigh scattering cross section remains relatively constant for a broad range of photon energies, whilst the Compton scattering peaks at a particular photon energy (~ 100 keV). Other interaction mechanisms exist [*e.g.* Delbrück (Papatzacos & Mort, 1975; Alvarez, Crawford & Stevenson, 1958), pair production, nuclear Thompson], but these do not become significant interaction processes for photon energies less than 1 MeV. This section will not address the interaction of photons with atoms for which the photon energy exceeds 100 keV.

4.2.3.1.3. *Normal attenuation, XAFS, and XANES*

The curves shown in Fig. 4.2.3.1 are the result of theoretical calculations of the interactions of an isolated atom with a single photon. Experiments are not usually performed on isolated atoms, however. When experiments are performed on ensembles of atoms, a number of points of difference emerge between the experimental data and the theoretical calculations. These effects arise because the presence of atoms in proximity with one another can influence the scattering process. In short: the total attenuation coefficient of the system is *not* the sum of all the individual attenuation coefficients of the atoms that comprise the system.

Perhaps the most obvious manifestation of this occurs when the photon energy is close to an absorption edge of an atom. In Fig. 4.2.3.2, the mass attenuation of several germanium compounds is plotted as a function of photon energy. The

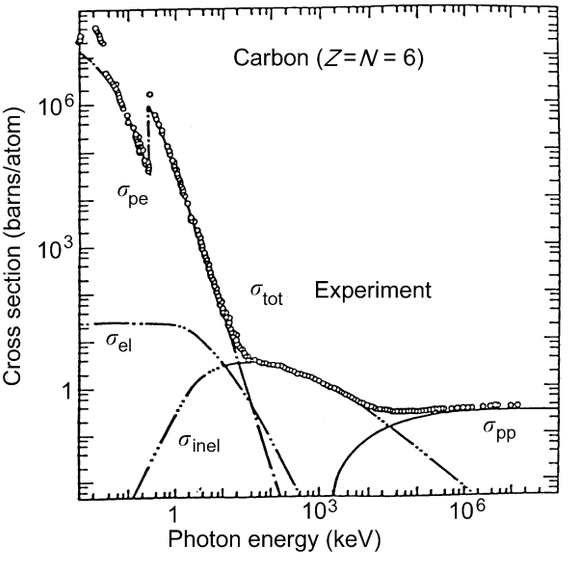

Fig. 4.2.3.1. Theoretical cross sections for photon interactions with carbon showing the contributions of photoelectric, elastic (Rayleigh), inelastic (Compton), and pair-production cross sections to the total cross sections. Also shown are the experimental data (open circles). From Gerstenberg & Hubbell (1982).

energy scale measures the distance from the *K*-shell edge energy of germanium (11.104 keV). These curves are taken from Hubbell, McMaster, Del Grande & Mallett (1974). Not only does the experimental curve depart significantly from the theoretically predicted curve, but there is a marked difference in the complexity of the curves between the various germanium compounds.

Far from the absorption edge, the theoretical calculations and the experimental data are in reasonable agreement with what one might expect using the sum rule for the various scattering cross sections and one could say that this region is one in which normal attenuation coefficients may be found.

Closer to the edge, the almost periodic variation of the mass attenuation coefficient is called the extended X-ray absorption fine structure (XAFS). Very close to the edge, more complicated fluctuations occur. These are referred to as X-ray absorption near edge fine structure (XANES). The boundary of the XAFS and XANES regions is somewhat arbitrary, and the physical basis for making the distinction between the two will be outlined in Subsection 4.2.3.4.

Even in the region where normal attenuation may be thought to occur, cooperative effects can exist, which can affect both the Rayleigh and the Compton scattering contributions to the total attenuation cross section. The effect of cooperative Rayleigh scattering has been discussed by Gerward, Thuesen, Stibius-Jensen & Alstrup (1979), Gerward (1981, 1982, 1983), Creagh & Hubbell (1987), and Creagh (1987*a*). That the Compton scattering contribution depends on the physical state of the scattering medium has been discussed by Cooper (1985).

Care must therefore be taken to consider the physical state of the system under investigation when estimates of the theoretical interaction cross sections are made.

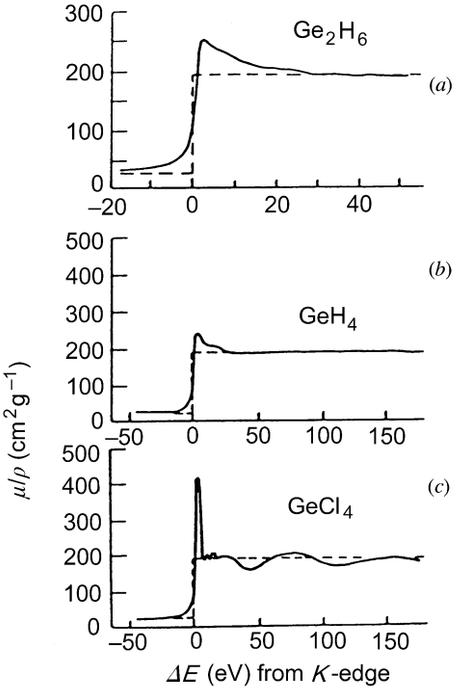

Fig. 4.2.3.2. The dependence of the X-ray attenuation coefficient on energy for a range of germanium compounds, taken in the neighbourhood of the germanium absorption edge (from *IT* IV, 1974).

4.2.3.2. *Techniques for the measurement of X-ray attenuation coefficients*

4.2.3.2.1. *Experimental configurations*

Experimental configurations that set out to determine the X-ray linear attenuation coefficient μ_l or the corresponding mass absorption coefficients (μ/ρ) must have characteristics that reflect the underlying assumptions from which equation (4.2.3.1) was derived, namely:

(i) the incident and transmitted beams are parallel and there is no divergence in the transmitted beam;

(ii) the photons in the incident and transmitted beams have the same energy;

(iii) the specimen is of sufficient thickness.

Because of the considerable discrepancies that often exist in X-ray attenuation measurements (see, for example, *IT* IV, 1974), the IUCr Commission on Crystallographic Apparatus set up a project to determine which, if any, of the many techniques for the measurement of X-ray attenuation coefficients is most likely to yield correct results. In the project, a number of different experimental configurations were used. These are shown in Fig. 4.2.3.3. The configurations used ranged in complexity from that

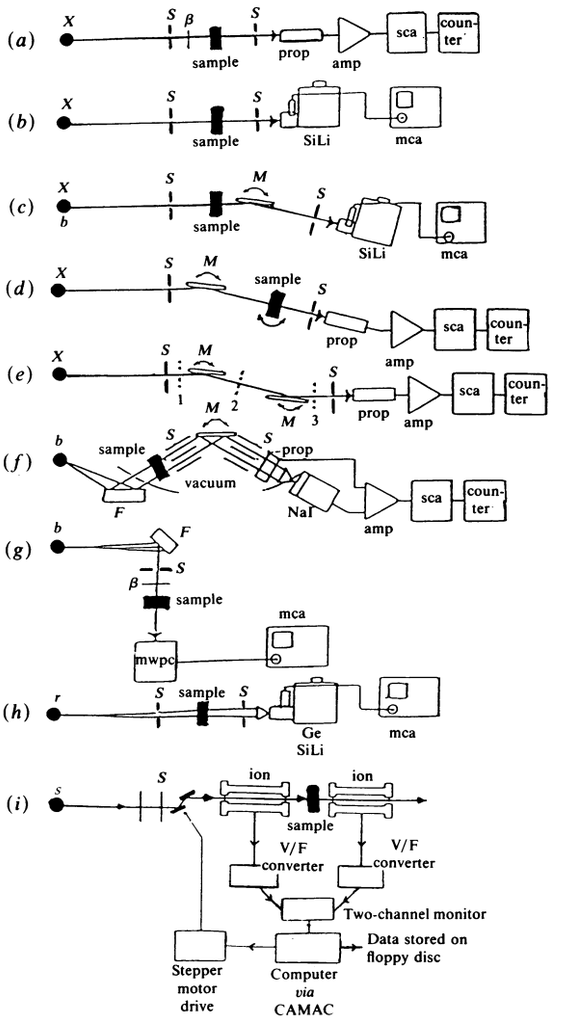

Fig. 4.2.3.3. Schematic representations of experimental apparatus used in the IUCr X-ray Attenuation Project (Creagh & Hubbell, 1987; Creagh, 1985). *X*: characteristic line from sealed X-ray tube; *b*: *Bremsstrahlung* from a sealed X-ray tube; *r*: radioactive source; *s*: synchrotron-radiation source; β: β-filter for characteristic X-rays; *S*: collimating slits; *M*: monochromator.

of Fig. 4.2.3.3(*a*), which uses a slit-collimated beam from a sealed tube and a β-filter to select its characteristic radiation, and a proportional counter and associated electronics to detect the transmitted-beam intensity, to that of Fig. 4.2.3.3(*f*), which uses a modification to a commercial X-ray-fluorescence analyser. Sources of X-rays included conventional sealed X-ray tubes, X-ray-fluorescence sources, radioisotope sources, and synchrotron-radiation sources. Detectors ranged from simple ionization chambers, which have no capacity for photon energy detection, to solid-state detectors, which provide a relatively high degree of energy discrimination. In a number of cases (Figs. 4.2.3.3*c*, *d*, *e*, and *f*), monochromatization of the beam was effected using single Bragg reflection from silicon single crystals. In Fig. 4.2.3.3(*i*), the incident-beam monochromator is using reflections from two Bragg reflectors tuned so as to eliminate harmonic radiation from the source.

The performance of these systems was evaluated for a range of materials that included:

(i) highly perfect silicon single crystals (Creagh & Hubbell, 1987);

(ii) polycrystalline copper foils that exhibited a high degree of preferred orientation; and

(iii) pyrolytic graphite that contained a high density of regular voids.

The results of this study are outlined in Section 4.2.3.2.3.

4.2.3.2.2. *Specimen selection*

Although the most important component in the experiment is the specimen itself, examination of the data files held at the US National Institute of Standards and Technology (Gerstenberg & Hubbell, 1982; Saloman & Hubbell, 1986; Hubbell, Gerstenberg & Saloman, 1986) has shown that, in general, insufficient care has been taken in the past to select an experimental device with characteristics that are appropriate to the specimen chosen. Nor has sufficient care been taken in the determination of the dimensions, homogeneity, and defect structure of the specimens. To achieve the best results, the following procedures should be followed.

(i) The *dimensions* of the specimen should be determined using at least two different techniques, and sample *thicknesses* should be chosen such that the Nordfors (1960) criterion, later confirmed by Sears (1983), that the condition

$$2 \leq \ln(I_0/I) \leq 4 \qquad (4.2.3.7)$$

be satisfied. This enables the best compromise between achieving good counting statistics and avoiding multiple photon scattering within the sample.

Wherever possible, different sample thicknesses should be chosen to enable a test of equation (4.2.3.1) to be made. If deviations from equation (4.2.3.1) exist, either the sample material or the experimental configuration, or both, are not appropriate for the measurement of μ_l. If the attenuation of the material under test falls outside the limits set by the Nordfors criterion and the material is in the form of a powder, the mixing of this powder with one with low attenuation and no absorption edge in the region of interest can be used to bring the total attenuation of the sample within the Nordfors range.

(ii) The sample should be examined by as many means as possible to ascertain its regularity, homogeneity, defect structure, and, especially for very thin specimens, freedom from pinholes and cracks. Where a diluent has been used to reduce the attenuation so that the Nordfors criterion is satisfied, care must be taken to ensure intimate mixing of the two materials and the absence of voids.

Since the theory upon which equation (4.2.3.1) is based envisages that each atom scatters as an individual, it is necessary to be aware of whether such cooperative effects as Laue–Bragg scattering (which may become significant in single-crystal specimens) and small-angle X-ray scattering (SAXS) (which may occur if a distribution of small voids or inclusions exists) occur in polycrystalline and amorphous specimens. Knowledge that cooperative scattering may occur influences the choice of collimation of the beam.

(iii) The sample should be mounted *normal* to the beam.

4.2.3.2.3. *Requirements for the absolute measurement of μ_l or (μ/ρ)*

The following prescription should be followed if accurate, absolute measurements of μ_l and (μ/ρ) are to be obtained.

(i) *X-ray source and X-ray monochromatization*. The *energy* of the incident photons should be measured directly using reflections from a single-crystal silicon monochromator, and the *energy spread* of the beam should be measured. Measurements should be made of the state of *polarization*, since X-ray-polarization effects are known to be significant in some measurements (Templeton & Templeton, 1982, 1985, 1986). The results of a survey on X-ray polarization were given by Jennings (1984). If a single-crystal monochromator is employed, it should be placed between the sample and the detector.

(ii) *Collimation*. It is of some advantage if both the incident-beam- and the transmitted-beam-defining slits can be varied in width.

Should it be necessary to combat the effects of Laue–Bragg scattering in a single-crystal specimen, an incident beam with a high degree of collimation is required (Gerward, 1981).

To counter the effects of small-angle X-ray scattering, it may be necessary to widen the detector aperture (Chipman, 1969). That these effects can be marked has been shown by Parratt, Porteus, Schnopper & Watanabe (1959), who investigated the influence collimator and monochromator configurations have on X-ray-attenuation measurements.

(iii) *Detection*. Detectors that give some degree of energy discrimination should be used. Compromise may be necessary between sensitivity and energy resolution, however, and these factors should be taken into account when a choice is being made between proportional and solid-state detectors.

Whichever detection system is chosen, it is essential that the system dead-time be determined experimentally. For descriptions of techniques for the determination of system dead-time, see, for example, Bertin (1975).

4.2.3.3. *Normal attenuation coefficients*

Fig. 4.2.3.1 shows that the X-ray attenuation coefficients are a smooth function of photon energy over a relatively large range of photon energies, and that discontinuities occur whenever the photon energy corresponds to a resonance in the electron cloud surrounding the nucleus. In Fig. 4.2.3.2, the effect of the interaction of the ejected photoelectron with the electron's neighbouring atoms is shown. Such edge effects (XAFS) can extend 1000 eV from the edge.

It is conventional, however, to extrapolate the smooth curve to the edge value, and a curve of *normal attenuation coefficients* results. These are taken to be the attenuation coefficients of the individual atoms. Tables of these *normal attenuation coefficients* are given in Section 4.2.4.

4.2.3.4. *Attenuation coefficients in the neighbourhood of an absorption edge*

4.2.3.4.1. *XAFS*

Although the existence of XAFS has been known for more than 60 years following experiments by Fricke (1920) and Hertz (1920), it is only in the last decade that a proper theoretical description has been developed. Kronig (1932*a*) suggested a long-range-order theory based on quantum-mechanical precepts, although later (Kronig, 1932*b*) he applied a short-range-order (SRO) theory to explain the existence of XAFS in molecular spectra. As time progressed, important suggestions were made by others, notably Kostarev (1941, 1949), who applied this SRO theory to condensed matter, Sawada, Tsutsumi, Shiraiwa, Ishimura & Obashi (1959), who accounted for the lifetime of the excited photoelectron and the core-hole state in terms of a mean free path, and Schmidt (1961*a*,*b*, 1963), who showed the influence atomic vibrations have on the phase of the back-scattered waves.

Nevertheless, neither the experimental data nor the theories were sufficiently good to enable Azaroff & Pease (1974) to decide which theory was the correct one to use. However, Sayers, Lytle & Stern (1970) produced a theoretical approach based on SRO theory, later extended by Lytle, Stern & Sayers (1975), and this is the foundation upon which all modern work has been built. Since 1970, a great deal of theoretical effort has been expended to improve the theory because of the need to interpret the wealth of data that became available through the increasing use of synchrotron-radiation sources in XAFS experiments.

A number of major reviews of XAFS theory and its use for the resolution of experimental data have been published. Contributions have been made by Stern, Sayers & Lytle (1975), Lee, Citrin, Eisenberger & Kincaid (1981), Lee (1981), and Teo (1981). The rapid growth of the use of synchrotron-radiation sources has led to the development of the use of XAFS in a wide variety of research fields. The XAFS community has met regularly at conferences, producing conference proceedings that demonstrate the maturation of the technique. The reader is directed to the proceedings edited by Mustre de Leon, Stern, Sayers, Ma & Rehr (1988), Hasnain (1990), and Kuroda, Ohta, Murata, Udagawa & Nomura (1992), and to the papers contained therein. In the following section, a brief, simplified, description will be given of the theory of XAFS and of the application of that theory to the interpretation of XAFS data.

4.2.3.4.1.1. *Theory*

The theory that will be outlined here has evolved through the efforts of many workers over the past decade. The oscillatory part of the X-ray attenuation relative to the 'background' absorption may be written as

$$\chi(E) = \frac{\mu_l(E) - \mu_{l0}(E)}{\mu_{l0}(E)}, \tag{4.2.3.8}$$

where $\mu_l(E)$ is the measured value of the linear attenuation coefficient at a photon energy E and $\mu_{l0}(E)$ is the 'background' linear attenuation coefficient. This is sometimes the extrapolation of the normal attenuation curve to the edge energy, although it is usually found necessary to modify this extrapolation somewhat to improve the matching of the higher-energy data with the XAFS data (Dreier, Rabe, Matzfeld & Niemann, 1984). In most computer programs, the normal attenuation curve is fitted to the data using cubic spline fitting routines.

The origin of XAFS lies in the interaction of the ejected photoelectron with electrons in its immediate vicinity. The wavelength of a photoelectron ejected when a photon is absorbed is given by $\lambda = 2\pi/k$, where

$$k = [(2m/\hbar^2)(E - E_0)]^{1/2}. \tag{4.2.3.9}$$

This outgoing spherical wave can be back-scattered by the electron clouds of neighbouring atoms. This back-scattered wave interferes with the outgoing wave, resulting in the oscillation of the absorption rate that is observed experimentally and called XAFS. Equation (4.2.3.8) was written with the assumption that the absorption rate was directly proportional to the linear absorption coefficient.

It is conventional to express $\chi(E)$ in terms of the momentum of the ejected electron, and the usual form of the theoretical expression for $\chi(\mathbf{k})$ is

$$\chi(\mathbf{k}) = \sum_i (N_i/kr_j^2)|f_i(k)| \exp(\sigma_i^2 k^2 - r_i/\rho) \sin[2kr_i + \varphi_i(k)]. \tag{4.2.3.10}$$

Here the summation extends over the shells of atoms that surround the absorbing atom, N_i representing the number of atoms in the ith shell, which is situated a distance r_i from the absorbing atom. The back-scattering amplitude from this shell is $f_i(k)$ for which the associated phase is $\varphi_i(k)$. Deviations due to thermal motions of the electrons are incorporated through a Debye–Waller factor, $\exp(-\sigma_i^2 k^2)$, and ρ is the mean free path of the electron.

The amplitude function $f_i(k)$ depends only on the type of back-scattering atom. The phase, however, contains contributions from both the absorber and the back-scatterer:

$$\varphi_i^l(k) = \varphi_j^l(k) + \varphi_i(k) - l\pi, \tag{4.2.3.11}$$

where $l = 1$ for K and $L_{\rm I}$ edges, and $l = 2$ or 0 for $L_{\rm II}$ and $L_{\rm III}$ edges. The phase is sensitive to variations in the energy threshold, the magnitude of the effect being larger for small electron energies than for electrons with considerable kinetic energy, *i.e.* the effect is more marked in the neighbourhood of the absorption edge. Since the position of the edge varies somewhat for different compounds (Azaroff & Pease, 1974), some impediment to the analysis of experimental data might occur, since the determination of the interatomic distance r_i depends upon the precise knowledge of the value of $\varphi_i(k)$.

In fitting the experimental data based on an empirical value of threshold energy using theoretically determined phase shifts, the difference between the theoretical and the experimental threshold energies ΔE_0 cannot produce a good fit at an arbitrarily chosen distance r_i, since the effect will be seen primarily at low k values ($\sim 0.3r\Delta E_0/k$), whereas changing r_i affects $\varphi_i(k)$ at high k values ($\sim 2k\Delta r$). This was first demonstrated by Lee & Beni (1977).

The significance of the Debye–Waller factor $\exp(-\sigma_i^2 k^2)$ should not be underestimated in this type of investigation. In XAFS studies, one is seeking to determine information regarding such properties of the system as nearest- and next-nearest-neighbour distances and the number of nearest and next-nearest neighbours. The theory is a short-range-order theory, hence deviations of atoms from their expected positions will influence the analysis significantly. Thus, it is often of value, experimentally, to work at liquid-nitrogen temperatures to reduce the effect of atomic vibrations.

Two distinct types of disorder are observed: vibrational, where the atom vibrates about a mean position in the structure, and static, where the atom occupies a position not expected theoretically. These terms can be separated from one

another if the variation of XAFS spectra with temperature is studied, because the two have different temperature dependences. A discussion of the effect of a thermally activated disorder that is large compared with the static order has been given by Sevillano, Meuth & Rehr (1978). For systems with large static disorders, *e.g.* liquids and amorphous solids, equation (4.2.3.10) has to be modified somewhat. The XAFS equation has to be averaged over the pair distribution function $g(r)$ for the system:

$$\chi(k) = \frac{F(k)}{k} \int_0^{\infty} g(r) \exp(-2r/\rho) \frac{\sin(2kr + \varphi_k)}{r^2} \, \mathrm{d}r. \quad (4.2.3.12)$$

Other factors that must be taken into account in XAFS analyses include: inelastic scattering (due to multiple scattering in the absorbing atom and excitations of the atoms surrounding the atom from which the photoelectron was ejected) and multiple scattering of the photoelectron. Should multiple scattering be significant, the simple model given in equation (4.2.3.10) is inappropriate, and more complex models such as those proposed by Pendry (1983), Durham (1983), Gurman (1988, 1995), Natoli (1990), and Rehr & Albers (1990) should be used. Several computer programs are now available commercially for use in personal computers (*EXCURVE*, *FEFF5*, *MSCALC*). Readers are referred to scientific journals to find how best to contact the suppliers of these programs.

4.2.3.4.1.2. *Techniques of data analysis*

Three assumptions must be made if XAFS data are to be used to provide accurate structural and chemical information:

(i) XAFS occurs through the interaction of waves *singly* scattered by neighbouring atoms;

(ii) the amplitude function of the atoms is insensitive to the type of chemical bond (the postulate of transferability), which implies that one can use the same amplitude function for a given atom in problems involving compounds of that atom, whatever the nature of its neighbours or the nature of the bond; and

(iii) the phase function can be transferred for each pair of absorber–back-scatterer atoms.

Of these three assumptions, (ii) is of the most questionable validity. See, for example, Stern, Bunker & Heald (1981).

It is usual, when analysing XAFS data, to search the literature for, or make sufficient measurements of, μ_{l0} remote from the absorption edge to produce a curve of $\mu_{l0}(E)$ *versus* E that can be extrapolated to the position of the edge. From equation (4.2.3.8), it is possible to produce a curve of $\chi(E)$ *versus* E from which the variation of $\chi(k)$ with k can be deduced using equation (4.2.3.9).

It is also customary to multiply $\chi(k)$ by some power of k to compensate for the damping of the XAFS amplitudes with increasing k. The power chosen is somewhat arbitrary but k^3 is a commonly used weighting function.

Two different techniques may be used to analyse the new data set, the *Fourier-transform technique* or the *curve-fitting technique*.

In the *Fourier-transform technique* (FF), the Fourier transform of the $k^n\chi(k)$ is determined for that region of momentum space from the smallest, k_1, to the largest, k_2, wavevectors of the photoelectron, yielding the radical distribution function $\rho_n(r')$ in coordinate (r') space.

$$\rho_n(r') = \frac{1}{(2\pi)^{1/2}} \int_{k_1}^{k_2} k^n \chi(k) \exp(i2kr') \, \mathrm{d}k. \quad (4.2.3.13)$$

The Fourier spectrum contains peaks indicating that the nearest-neighbour, next-nearest-neighbour, *etc.* distances will differ from the true spacings by between 0.2 to 0.5 Å depending on the elements involved. These position shifts are determined for model systems and then *transferred* to the unknown systems to predict interatomic spacings. Fig. 4.2.3.4 illustrates the various steps in the Fourier-transform analysis of XAFS data.

The technique works best for systems having well separated peaks. Its primary weakness as a technique lies in the fact that the phase functions are not linear functions of k, and the spacing shift will depend on E_0, the other factors including the weighting of data before the Fourier transforms are made, the range of k space transformed, and the Debye–Waller factors of the system.

In the *curve-fitting technique* (CF), least-squares refinement is used to fit the spectra in k space using some structural model for the system. Such techniques, however, can only indicate which of several possible choices is more likely to be correct, and *do not prove* that that structure is the correct structure.

It is possible to combine the FF and CF techniques to simplify the data analysis. Also, for data containing single-scatter peaks, the phase and amplitude components can be separated and analysed separately using either theory or model compounds (Stern, Sayers & Lytle, 1975).

Each XAFS data set depends on two sets of strongly correlated variables: $\{F(k), \sigma, \rho, N\}$ and $\{\varphi(k), E_0, r\}$. The elements of each set are not independent of one another. To determine N and σ,

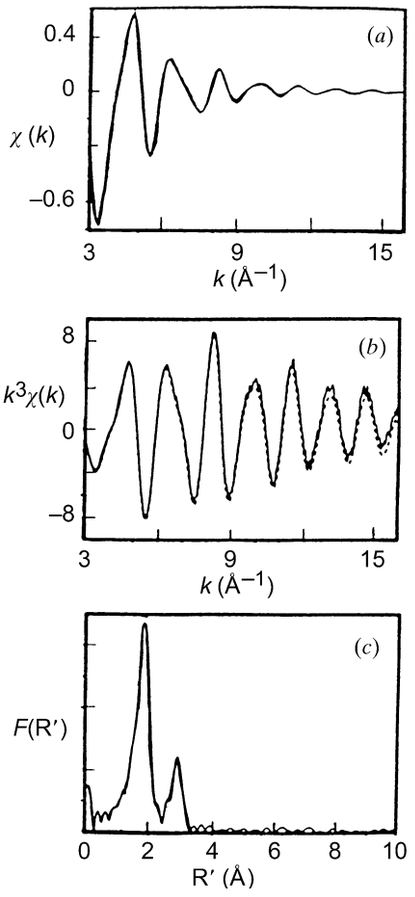

Fig. 4.2.3.4. Steps in the reduction of data from an XAFS experiment using the Fourier transform technique: (*a*) after the removal of background $\chi(k)$ *versus* k; (*b*) after multiplication by a weighting function (in this case k^3); (*c*) after Fourier transformation to determine r'.

one must know $F(k)$ well. To determine r, $\varphi(k)$ must be known accurately.

Attempts have been made by Teo & Lee (1979) to calculate $F(k)$ and $\varphi(k)$ from first principles using an electron–atom scattering model. Parametrized versions have been given by Teo, Lee, Simons, Eisenberger & Kincaid (1977) and Lee *et al.* (1981). Claimed accuracies for r, σ, and N in XAFS determinations are 0.5, 10, and 20%, respectively.

Acceptable methods for data analysis must conform to a number of basic criteria to have any validity. Amongst these are the following:

(i) the data analysis must not give rise to systematic error in the sense that it must provide unbiased estimates of parameters;

(ii) the assumed (hypothetical) model must be able to describe the data adequately;

(iii) the number of parameters used to describe the best fit of data must not exceed the number of independent data points;

(iv) where multiple solutions exist, supplementary information or assumptions used to resolve the ambiguity must conform to the philosophy of choice of the model structure.

The techniques for estimation of the parameters must always be given, including all known sources of uncertainty.

A complete list of criteria for the correct analysis and presentation of XAFS data is given in the reports of the International Workshops on Standards and Criteria in XAFS (Lytle, Sayers & Stern, 1989; Bunker, Hasnain & Sayers, 1990).

4.2.3.4.1.3. *XAFS experiments*

The variety and number of experiments in which XAFS experiments have been used is so large that it is not possible here to give a comprehensive list. By consulting the papers given in such texts as those edited by Winick & Doniach (1980), Teo & Joy (1981), Bianconi, Incoccia & Stipcich (1983), Mustre de Leon *et al.* (1988), Hasnain (1990), and Kuroda *et al.* (1992), the reader may find references to a wide variety of experiments in fields of research ranging from archaeology to zoology.

In *crystallography*, XAFS experiments have been used to assist in the solution of crystal structures; the large variations in the atomic scattering factors can be used to help solve the phase problem. Helliwell (1984) reviewed the use of these techniques in protein crystallography. A further discussion of the use of these anomalous-dispersion techniques in crystallography has been given by Creagh (1987*b*). The relation that exists between the attenuation (related to the imaginary part of the dispersion correction, f'') and intensity (related to the atomic form factor and the real part of the dispersion correction, f') is discussed by Creagh in Section 4.2.6. Specifically, modulations occur in the observed diffracted intensities from a specimen as the incident photon energy is scanned through the absorption edge of an atomic species present in the specimen. This technique, referred to as diffraction anomalous fine structure (DAFS) is complementary to XAFS. Because of the dependence of intensity on the geometrical structure factor, and the fact that the structure factor itself depends on the positional coordinates of the absorbing atom, it is possible to discriminate, in some favourable cases, between the anomalous scattering between atoms occupying different sites in the unit cell (Sorenson *et al.*, 1994).

In many systems of *biological* interest, the arrangement of radicals surrounding an active site must be found in order that the role of that site in biochemical processes may be assessed. A study of the XAFS spectrum of the active atom yields structural information that is specific to that site. Normal crystallographic techniques yield more general information concerning the crystal structure. An example of the use of XAFS in biological systems is the study of iron–sulfur proteins undertaken by Shulman, Weisenberger, Teo, Kincaid & Brown (1978). Other, more recent, studies of biological systems include the characterization of the Mn site in the photosynthetic oxygen evolving complexes including hydroxylamine and hydroquinone (Riggs, Mei, Yocum & Penner-Hahn, 1993) and an XAFS study with an *in situ* electrochemical cell on manganese Schiff-base complexes as a model of a photosystem (Yamaguchi *et al.*, 1993).

It must be stressed that the theoretical expression (equation 4.2.3.10) does not take into account the state of polarization of the incident photon. Templeton & Templeton (1986) have shown that polarization effects may be observed in some materials, *e.g.* sodium bromate. Given that most XAFS experiments are undertaken using the highly polarized radiation from synchrotron-radiation sources, it is of some importance to be aware of the possibility that dichroic effects may occur in some specimens.

Because XAFS is a short-range-order phenomenon, it is particularly useful for the structural study of such *disordered systems* as liquid metals and amorphous solids. The analysis of such disordered systems can be complicated, particularly in those cases where excluded-volume effects occur. Techniques for analysis for these cases have been suggested by Crozier & Seary (1980). Fuoss, Eisenberger, Warburton & Bienenstock (1981) suggested a technique for the investigation of amorphous solids, which they call the differential anomalous X-ray scattering (DAS) technique. This method has some advantages when compared with conventional XAFS methods because it makes more effective use of low-k information, and it does not depend on a knowledge of either the electron phase shifts or the mean free paths.

Both the conventional XAFS and DAS techniques may be used for studies of surface effects and catalytic processes such as those investigated by Sinfelt, Via & Lytle (1980), Hida *et al.* (1985), and Caballero, Villain, Dexpert, Le Peltier & Lynch (1993).

It must be stressed that in all the foregoing discussion it has been assumed that the detection of XAFS has been by measurement of the linear attenuation coefficient of the specimen. However, the process of photon absorption followed by the ejection of a photoelectron has as its consequence both *X-ray fluorescence* and *surface XAFS* (SEXAFS) and *Auger electron emission*. All of these techniques are extremely useful in the analysis of dilute systems.

SEXAFS techniques are extremely sensitive to surface conditions since the mean free path of electrons is only about 20 Å. Discussions of the use of SEXAFS techniques have been given by Citrin, Eisenberger & Hewitt (1978) and Stohr, Denley & Perfettii (1978). A major review of the topic is given in Lee *et al.* (1981). SEXAFS has the capacity of sensing thin films deposited on the surface of substrates, and has applications in experiments involving epitaxic growth and absorption by catalysts.

Fluorescence techniques are important in those systems for which the absorption of the specimen under investigation contributes only very slightly to the total attenuation coefficient since it detects the fluorescence of the absorbing atom directly. Experiments by Hastings, Eisenberger, Lengeler & Perlman (1975) and Marcus, Powers, Storm, Kincaid & Chance (1980) proved the importance of this technique in analysing dilute alloy and biological specimens. Materlik, Bedzyk & Frahm (1984) have demonstrated its use in determining the location of bromine atoms absorbed on single-crystal silicon substrates. Oyanagi, Matsushita, Tanoue, Ishiguro & Kohra (1985) and Oyanagi, Takeda, Matsushita, Ishiguro & Sasaki (1986) have also used fluorescence XAFS techniques for the characterization of very

Table 4.2.3.1. *Some synchrotron-radiation facilities providing XAFS databases and analysis utilities*

Country	Synchrotron source	Address
France	LURE	Université Paris-Sud, LURE, 91405 Orsay, France
Italy	Frascati	Laboratori Nationali di Frascati, CP 13, 00044 Frascati, Italy
Japan	Photon Factory	Photon Factory, National Laboratory for High Energy Physics, 1-1 Oho, Tsukuba-gun, Ibaraki 305, Japan
Germany	DESY	DESY, Notkestrasse 85, 2000 Hamburg 52, Germany
United Kingdom	SRC/ Daresbury	Daresbury Laboratory, Daresbury, Warrington WA4 4AD, England
USA	CHESS	CHESS, Cornell University, Ithaca, New York 14853, USA
	NSLS	NSLS, Brookhaven National Laboratory, Upton, New York 11973, USA
	SPEAR	SSRL, Stanford University, Bin 69, PO Box 4349, Stanford, California 94305, USA

thin films. More recently, Oyanagi *et al*. (1987) have applied the technique to the study of short-range order in high-temperature superconductors. Oyanagi, Martini, Saito & Haga (1995) have studied in detail the performance of a 19-element high-purity Ge solid-state detector array for fluorescence X-ray absorption fine structure studies.

A less-sensitive technique, but one that can be usefully employed for thin-film studies, is that in which XAFS modulations are detected in the beam reflected from a sample surface. This technique, *ReflEXAFS*, has been used by Martens & Rabe (1980) to investigate superficial regions of copper oxide films by means of reflection of the X-rays close to the critical angle for total reflection.

If a thin film is examined in a transmission electron microscope, the electron beam loses some of its kinetic energy in interactions between the electron beam and the electrons within the film. If the resultant energy loss is analysed using a magnetic analyser, XAFS-like modulations are observed in the electron energy spectrum. These modulations, electron-energy-loss fine structure (*EELS*), which were first observed in a conventional transmission electron microscope by Leapman & Cosslet (1976), are now used extensively for microanalyses of light elements incorporated into heavy-element matrices. Most major manufacturers of transmission electron microscopes supply electron-energy-loss spectrometers for their machines. There are more problems in analysing electron-energy-loss spectra than there are for XAFS spectra. Some of the difficulties encountered in producing reliable techniques for the routine analysis of EELS have been outlined by Joy & Maher (1985). This matter is discussed more fully in §4.3.4.4.2.

A more recent development has been the observation of *topographic XAFS* (Bowen, Stock, Davies, Pantos, Birnbaum & Chen, 1984). This fine structure is observed in white-beam topographs taken using synchrotron-radiation sources. The technique provides the means of simultaneously determining spatially resolved microstructural and spectroscopic information for the specimen under investigation.

In all the preceeding discussion, however, the electron was assumed to undergo only single-scattering processes. If multiple scattering occurs, then the theory has to be changed somewhat. §4.2.3.4.2 discusses the effect of multiple scattering.

4.2.3.4.2. *X-ray absorption near edge structure (XANES)*

In Fig. 4.2.3.2(*c*), there appears to be one cycle of strong oscillation in the neighbourhood of the absorption edge before the quasi-periodic variation of the XAFS commences. The electrons that cause this strong modulation of the photoelectric scattering cross section have low k values, and the electron is strongly scattered by neighbouring atoms. It was mentioned in §4.2.3.4.1 that conventional XAFS theory assumes a weak, single-scattering interaction between the ejected photoelectron and its environment. A schematic diagram illustrating the difference between single- and multiple-scattering processes is given in Fig. 4.2.3.5. Evidently, the multiple-scattering process is very complicated and a discussion of the theory of XANES is too complex to be given here. The reader is directed to papers by Pendry (1983), Lee (1981), and Durham (1983). A more recent review of the study of fine structure in ionization cross sections and their use in surface science has been given by Woodruff (1986).

The data from XANES experiments can be analysed to determine structural information such as coordination geometry, the symmetry of unoccupied valence electronic states, and the effective charge on the absorbing atom (Natoli, Misemer, Doniach & Kutzler, 1980; Kutzler, Natoli, Misemer, Doniach & Hodgson, 1981). XANES experiments have been performed to resolve many problems, *inter alia*: the origin of white lines (Lengeler, Materlik & Müller, 1983); absorption of gases on metal surfaces (Norman, Durham & Pendry, 1983); the effect of local symmetry in 3*d* elements (Petiau & Calas, 1983); and the determination of valence states in materials (Lereboures, Dürr, d'Huysser, Bonelle & Lenglet, 1980).

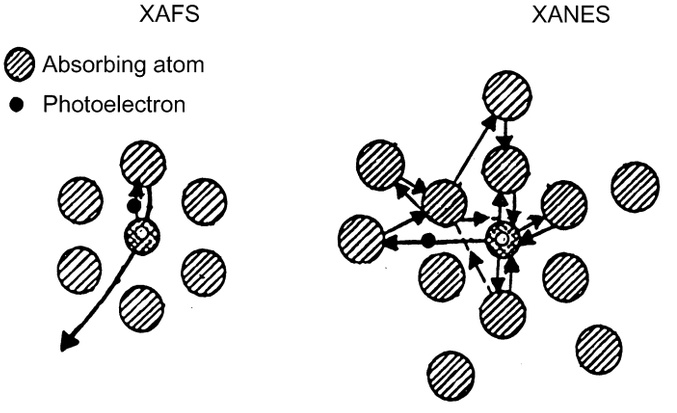

Fig. 4.2.3.5. Schematic representations of the scattering processes undergone by the ejected photoelectron in the single-scattering (XAFS) case and the full multiple-scattering regime (XANES).

4.2.3.5. *Comments*

For reliable experiments using XAFS and XANES to be undertaken, intense-radiation sources must be used. Synchrotron-radiation sources are such a source of highly intense X-rays. Their ready availability to experimenters and the comparative simplicity of the equipment required to perform the experiments have made experiments involving XAFS and XANES very much easier to perform than has hitherto been the case.

At some synchrotron-radiation sources, database and program libraries for the storage and analysis of XAFS and XANES data exist. These are usually part of the general computing facilities (Pantos, 1982).

Crystallographers seeking information concerning the nature and extent of these computer facilities can find such information by contacting the computer centre at one of the synchrotron-radiation establishments listed in Table 4.2.3.1.

4.2.4. X-ray absorption (or attenuation) coefficients (By D. C. Creagh and J. H. Hubbell)

4.2.4.1. *Introduction*

This data set is intended to supersede those data sets given in *International Tables for X-ray Crystallography*, Vols. III (Koch, MacGillavry & Milledge, 1962) and IV (Hubbell, McMaster, Del Grande & Mallett, 1974).

It is not intended here to give a detailed bibliography of experimental data that have been obtained in the past 90 years. This has been the subject of a number of publications, *e.g.* Saloman & Hubbell (1987), Hubbell, Gerstenberg & Saloman (1986), Saloman & Hubbell (1986), and Saloman, Hubbell & Scofield (1988). Further commentary on the validity and the quality of the experimental data in existing tabulations has been given by Creagh & Hubbell (1987) and Creagh (1987).

Existing tabulations of X-ray attenuation (or absorption) cross sections fall into three distinct categories: purely theoretical, purely experimental, and an evaluated mixture of theoretical and experimental data.

Compilations of the purely theoretically derived data exist for:

photo-effect absorption cross sections (Storm & Israel, 1970; Cromer & Liberman, 1970; Scofield, 1973; Hubbell, Veigele, Briggs, Brown, Cromer & Howerton, 1975; Band, Kharitonov & Trzhaskovskaya, 1979; Yeh & Lindau, 1985);

Compton scattering cross sections (Hubbell *et al.*, 1975);

Rayleigh scattering cross sections (Hubbell *et al.*, 1975; Hubbell & Øverbø, 1979; Schaupp, Schumacher, Smend, Rullhausen & Hubbell, 1983).

Many purely experimental compilations exist, and the cross-section data given in computer programs used in the analysis of results in X-ray-fluorescence spectroscopy, electron-probe microanalysis, and X-ray diffraction are usually (evaluated) compilations of several of the following compilations: Allen (1935, 1969), Victoreen (1949), Liebhafsky, Pfeiffer, Winslow & Zemany (1960), Koch *et al.* (1962), Heinrich (1966), Theisen & Vollath (1967), Veigele (1973), Leroux & Thinh (1977), Montenegro, Baptista & Duarte (1978), and Plechaty, Cullen & Howerton (1981). If a comparison is made between these data sets, significant discrepancies are found, and questions must be asked concerning the reliability of the data sets that are compared. Jackson & Hawkes (1981) and Gerward (1986) have produced sets of parametric tables to simplify the application of X-ray attenuation data for the solution of problems in computer-aided tomography and X-ray-fluorescence analysis.

Compilations by Henke, Lee, Tanaka, Shimambukuro & Fujikawa (1982) and the earlier tables of McMaster, Del Grande, Mallett & Hubbell (1969/1970) are examples of the judicious application of both theoretical and experimental data to produce a comprehensive data set of X-ray interaction cross sections.

Because of the discrepancies that appear to exist between experimental data sets, the IUCr Commission on Crystallographic Apparatus set up a project to establish which, if any, of the existing methods for measuring X-ray interaction cross sections (X-ray attenuation coefficients) and which theoretical calculations could be considered to be the most reliable. A discussion of some of the major results of this project is given in Section 4.2.3. A more detailed description of this project has been given by Creagh & Hubbell (1987, 1990).

In this section, tabulations of the total X-ray interaction cross sections σ and the mass absorption coefficient μ_m are given for a range of characteristic X-ray wavelengths [Ti $K\alpha$ 2.7440 Å (or 4.509 keV) to Ag $K\beta$ 0.4470 Å (or 24.942 keV)]. The interaction cross sections are expressed in units of barns/atom (1 barn $= 10^{-28}$ m^2) whilst the mass absorption coefficient is given in cm^2 g^{-1}. Table 4.2.4.1 sets out the wavelengths of the characteristic wavelengths used in Tables 4.2.4.2 and 4.2.4.3, which list values of σ and μ_m, respectively.

Users of these tables should be aware of three important facts.

(i) The values given in the tables are derived for the case of isolated atoms, and cooperative effects may become important in condensed phases (Section 4.2.3).

(ii) The values are based solely on theoretical calculations.

(iii) The limits to the reliability of the data when compared with experimental values are shown in Fig. 4.2.4.4.

The linear attenuation coefficient μ_l in units of cm^{-1} can be defined operationally as

$$\mu_l = \left(\ln \frac{I_o}{I}\right) \Big/ t \qquad (4.2.4.1)$$

from the exponential attenuation relationship

$$\frac{I}{I_0} = \exp(-\mu_l t) \qquad (4.2.4.2)$$

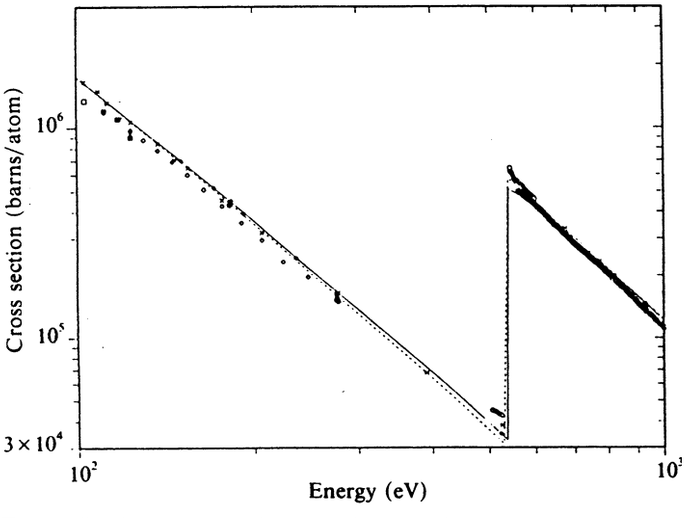

Fig. 4.2.4.1. Agreement between theory and experiment for oxygen ($Z = 8$) in the 'soft' X-ray region. The solid line is for the Scofield (1973) values without renormalization and the dotted line is for the semi-empirical data of Henke *et al.* (1982).

references